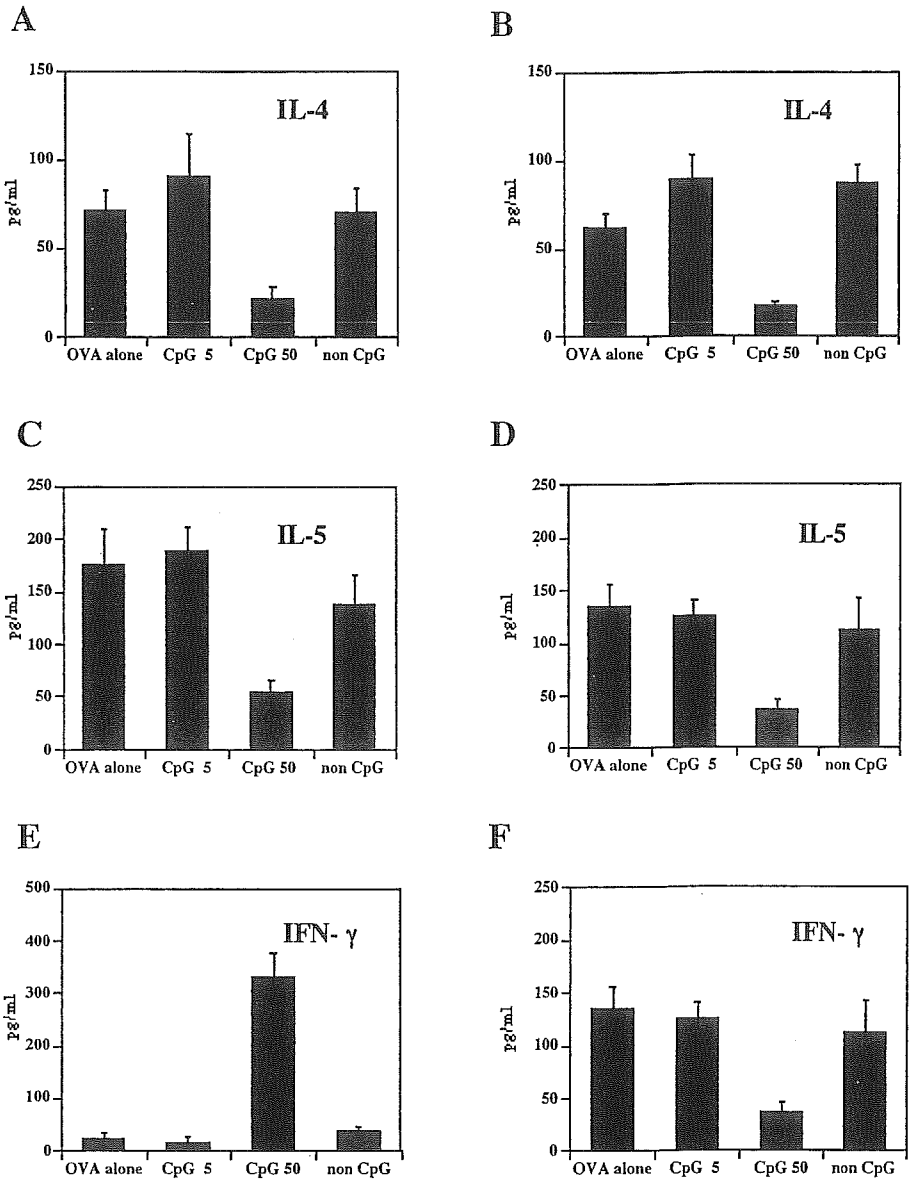

FIG. 5. Cytokine production by nasal mononuclear cells from mice immunized with CpG in vitro. Mice were immunized with OVA alone, OVA+CpG 5 μg and 50 μg CpG or OVA+non-CpG. Those cells were collected from two noses of mice and cultured for 72 h with OVA, then the supernatants were analyzed by sandwich ELISA. Results show the mean±SEM from triplicate wells. Detection limit for IL-4, IL-5, IFN-γ was 15, 20, and 20 pg/ml, respectively.

mediated eosinophilic inflammation and symptoms in a murine model of allergic rhinitis (26). Many other studies also showed that co-administration of CpG with anitigens suppressed the initiation and exacerbation of allergic disease in murine models. A new finding in our study was the strain difference in the optimal dose of CpG for preventing Th 2 responses. We dem-

onstrated that intranasal immunization of OVA plus CpG could suppress Th 2 immune response in two different mouse strains, but the two mouse strains showed different profiles of CpG-induced immunoalteration.

BALB/c mice displayed marked elevation of IgG 2 a production when 50 μg CpG was administered, while C 57 BL/6 mice showed only a little enhancement. On the other hand, levels of IgG 1 were not statistically different between the two mice strains. Some experiments demonstrated that CpG immunization did not necessarily downregulate IgG 1 production. Our data is consistent with these reports. OVA-specific IgE production was decreased significantly in both mouse strain. In BALB/c mice, the suppressive effect of CpG on IgE production was less active than that in C 57 BL/6 mice. Moreover, downregulation of Th 2 cytokine production by nasal lymphocytes immunized with OVA plus CpG was stronger than that in C 57 BL/6 mice. Th 1 cytokine (IFN-γ) production was also increased in BALB/c compared with that in C 57 BL/6. Furthermore, we demonstrated that nasal lymphocytes from BALB/c mice produced significantly higher levels of Th 1 cytokine IL-12 than those from C 57 BL/6 mice after stimulation with CpG in vitro. Taken together, our experiments indicate that CpG treatment seems to be more effective in BALB/c mice compared with C 57 BL/6 mice.

Previous studies demonstrated the strain difference in the susceptibility to intranasal immunization in mice. Okano et al. showed that intranasal administration with the egg antigen of *Schistosoma mansoni* induced strong Th 2 response in strain-dependent manner (27). Tamura et al. showed that BDF 1 mice were high responders compared with other strains during the intranasal immunization with OVA with cholera toxin B subunit (28). The reason is not clear why the difference of ability to suppress the Th 2 immune response between the two mice strains had been occurred. It has been well known that CpG-DNA activate dendritic cell (DC) characterized by cytokine (IL-12, TNF-α) production, co-stimulatory molecules, and an increased ability to activate Tcells through Toll like receptor (TLR 9). If the difference was in proportion to the expression levels of TLR 9, BALB/c mice have higher levels of TLR 9 than C 57 BL/6. However, Liu et al. demonstrated that the expression levels of TLR 9 mRNA were higher in DC isolated from the spleens of native BALB/c mice than in those from C 57 BL/6 mice (31). This result is not consistent with our present results. We suppose that the specification of mucosal immunity was large due to the contradiction. For example, naso-associated lymphoid tissue (NALT) and gut-associated lymphoid tissue (GALT) have B 1 cells that differentiate to IgA-producing cells and γδ Tcells that contributes to the activation of primitive response to bacterial infections (29). Moreover, Iwasaki et al. reported that CD 11

b-CD 8-dendritic cells (DC) are localized in Peyers patch (30). Further studies were needed to conclude the exact mechanism.

Route of immunization with CpG was intranasal application in our present study. Nasal lymphocytes from OVA/CpG-immunized mice produced significant levels of IFN-γ in response to re-stimulation with OVA. The ability of nasal lymphocytes to induce Th 1 response in vitro suggests that these cells may be the effector cells responsible for induction of Th 1. In many studies, splenic mononuclear or lymph node cells have been used to investigate the cytokine profiles in vitro. Those cells might be suitable to examine the systemic immune response, however, not to investigate the local immune response such as the case of mucosal immunity. Local application of CpG will be hopeful for the prevention of allegic rhinitis in future.

In summary, we demonstrated that the immunomodulating effect of CpG on Th 2 response was different between C 57 BL/6 and BALB/c mice. What we should learn from the murine study is the presence of dose variety to obtain optimal effects of CpG under the respective genetic background. These results have implications for development of CpG-based immunotherapy in allergic disease in humans.

ACKNOWLEDGEMENTS

This study was supported in part by Grant-in-Aid of Scientific Research, Japan Society for the promotion of Science (#15390137).

REFERENCES

1. Romagnani S. Regulation of the development of type 2 T-helper cells in allergy. *Curr Opinion Immunol* 1994; **6** : 838-46.
2. Durham SR, Ying S, Varney VA, Jacobson MR, Sudderick RM, Mackay IS, *et al.* Cytokine messenger RNA expression for IL-3, IL-4, IL-5, and granulocyte/macrophage colonu-stimulating factor in the nasal mucosa after local allergen provocation: Relationship to tissue eosinophilia. *J Immunol* 1992; **148** : 2390-4.
3. Seder RA, Paul WE. Acquisition of lymphokine-producing phenotype by CD 4+T cells. *Annu Rev Immunol* 1994; **12** : 635-73.
4. Mosmann TR, Sad S. The expanding universe of T-cell subsets: Th 1, Th 2 and more. *Immunol Today* 1996; **17** : 138-46.
5. Secrist H, Chelen CJ, Wen Y, Marshall JD, Umetsu DT. Allergen immunotherapy decreases tinterleukin 4 production tin CD 4+T cells from allergic tindividuals. *J Exp Med* 1988; **167** : 219-24.

6. Snapper CM, Paul WE. Interferon-g and B cell stimulatory factor-1 reciprocally regulate Ig Isotype production. *Science* 1987; **236** : 944-7.
7. Noon L. Prophylactic inoculation against hay fever. *Lancet* 1911; **1** : 1572.
8. Manichan E, Rouse RJ, Yu Z, Wire WS, Rouse BT. Genetic immunization against herpes simplex virus. Protection is mediated by CD 4+T lymphocytes. *J Immunol* 1995; **155** : 259-65.
9. Leclerc C, Deriand E, Rojas M, Whalen RG. The preferential induction of a Th 1 immune response by DNA-based immunization is mediated by the immunostimulatory effect of plasmid DNA. *Cell Immunol* 1999; **103** : 107-13.
10. Sato Y, Roman M, Tighe H, *et al.* Immunostimulatory DNA sequences necessary for effective intradermal immunization. *Science* 1996; **273** : 352-4.
11. Roman M, M-Orozco E, Goodman JS, Nguyen M-D, Malek S, *et al*. Immunostimulatory DNA sequences function as T helper-1 promoting adjuvants. *Nat Med* 1997; **3** : 849-54.
12. Sparwasser T, Koch ES, Vabulas RM, *et al*. Bacterial DNA and immunostimulatory CpG oligodeoxynucleotides trigger maturation and activation of murine dendritic cells. *Eur J Immunol* 1998; **28** : 2045-54.
13. Bohle B, Jahn-Schmid B, Maurer D, Kraft D, Ebner C. Oligodeoxynucleotides containing CpG motifs induce IL-12, IL-18 and IFN-γ production in cells from allergic individuals and inhibit IgE synthesis. *Eur J Immunol* 1999; **161** : 4493-7.
14. Kline JN, Waldschmidt TJ, Businga TR, *et al*. Modulation of airway inflammation by CpG oligodeoxynucleotides in a murine model of asthma. *J Immunol* 1998; **160** : 2555-9.
15. Broide D, Schwarze J, Tighe H, *et al*. Immunostimulatory DNA sequences inhibit IL-5, eosinophilic inflammation, and airqway hyperresponsiveness in mice. *J Immunol* 1998; **161** : 7054-62.
16. Beatrice JS, Ursula W, Barbara B, *et al*. Oligodeoxynucleotides containing CpG motifs modulates the allergic TH 2 response of BALB/c mice to Bet v 1, the major birch pollen allergen. *J Allergy Clin Immunol* 1999; **104** : 1015-23.
17. Kohama Y, Akizuki O, Hagihara K, *et al*. Immunostimulatory Oligodeoxynucleotide induces TH 1 immune response and inhibition of IgE antibody production to cedar pollen allergens in mice. *J Allergy Clin Immunol* 1999; **104** : 1231-8.
18. Shirota H, Sano K, Kikuchi T, *et al*. Regulation of murine airway eosinophilia and Th 2 cells by antigen-congugated CpG oligodeoxynucleotides as a novel antigen-specific immunomodulator. *J Immunol* 2000; **164** : 5575-5582.
19. Tighe H, Takabayashi K, Schwarts D, *et al*. Coupling CpG motif immunostimulatory DNA to ragweed allergen Amb a 1 tinduces a Th 1 response to allergen. J *Allergy Clin Immunol* 1999; **103** : S 48.
20. Tighe H, Takabayashi K, Schwarts D, *et al*. Conjugation of immunostimulatory DNA to the short ragweed allergen Amb a 1 enhances its immunogenicity and reduces its allergenicity. *J Allergy Clin Immunol* 2000; **106** : 124-34.
21. Tulic MK, Fiset PO, Chiristodoulopoulos P, *et al*. Amb a 1-immunostimulatory oligodeoxynucleotide conjugate immunotherapy decreases the nasal inflammatory response. *J Allergy Clin Immunol* 2003; **113**

: 235-242.

22. Okano M, Satoskar AR, Nishizaki K, *et al*. Induction of Th 2 responses and IgE is largely due to carbohydrates functioning as adjuvants on *Schistosoma mansoni* egg antigens. *J Immunol* 1999; **15** : 6712-7.
23. Asanuma H, Inaba Y, Aizawa C, *et al*. Characterization of mouse nasal lymphocytes isolated by enzymatic extraction with collagenase. *J Immunol Methods* 1995; **187** : 41-51
24. Okano M, Satoskar AR, Nishizaki K, *et al*. Lacto-N-fucopentaose 3 found on *Schistosoma mansoni* egg antigens functions as adjuvant for proteins by inducing Th 2-type response. *J Immunol* 2001; **167** : 442.
25. Takabayashi K, Libet L, Chisholm D, Zubeldia J, Horner A. Intranasal immunotherapy is more effective than intradermal immunotherapy for the induction of airway allergen tolerance in Th 2-sensitized mice. *J Immunol* 2003; **170** : 3898-905.
26. Hussain I, Jain VV, Kitagaki K. Modulation of murine allergic rhinosinusitis by CpG oligodeoxynucleotides. *Laryngoscope* 2002; **112** : 1819-26.
27. Okano M, Nishizaki K, Abe M. Strain-dependent induction of allergic rhinitis without adjuvant in mice. *Allergy* 1999; **54** : 593-601.
28. Tamura S, Shoji Y, Hashiguchi K. Effects of cholera toxin adjuvant on IgE antibody response to orally or nasally administered ovalbumin. *Vaccine* 1994; **12** : 1238-40.
29. Kelsall B, Strober W. Gut-associated lymphoid tissue. Antigen handling and T lymhocyte responses. Academic Press, *San Diego*, 1999, 293-317.
30. Iwasaki A, Kelsall BL. Freshly isolated Peyer's patch, but not spleen, dendritic cells produce interleukin 10 and induce the differentiation of T helper type 2 cells. *J Exp Med* 1999; **190** : 229-239.
31. Liu T, Matsuguchi T, Tsuboi N, *et al.* Differences in expression of Toll-like receptors and their reactivities in dendritic cells in BALB/c and C 57 BL/6 mice. *Infect Immun* 2002; **70** : 6638-45.

Acta Crystallographica Section F
Structural Biology and Crystallization Communications
ISSN 1744-3091

Expression, purification and crystallization of *Trypanosoma cruzi* dihydroorotate dehydrogenase complexed with orotate

Daniel Ken Inaoka,[a] Eizo Takashima,[a] Arihiro Osanai,[a] Hironari Shimizu,[a] Takeshi Nara,[b] Takashi Aoki,[b] Shigeharu Harada[c] and Kiyoshi Kita[a]*

[a]Department of Biomedical Chemistry, Graduate School of Medicine, The University of Tokyo, 7-3-1 Hongo, Bunkyo-ku, Tokyo 113-0033, Japan, [b]Department of Parasitology, Juntendo University, 2-1-1 Hongo, Bunkyo-ku, Tokyo 113-8421, Japan, and [c]Department of Applied Biology, Kyoto Institute of Technology, Sakyo-ku, Kyoto 606-8585, Japan

Correspondence e-mail: kitak@m.u-tokyo.ac.jp

Received 2 June 2005
Accepted 19 August 2005
Online 13 September 2005

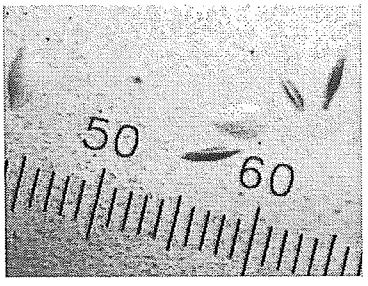

Dihydroorotate dehydrogenase (DHOD) catalyzes the oxidation of dihydroorotate to orotate, the fourth step and the only redox reaction in the *de novo* biosynthesis of pyrimidine. DHOD from *Trypanosoma cruzi* (TcDHOD) has been expressed as a recombinant protein in *Escherichia coli* and purified to homogeneity. Crystals of the TcDHOD–orotate complex were grown at 277 K by the sitting-drop vapour-diffusion technique using polyethylene glycol 3350 as a precipitant. The crystals diffract to better than 1.8 Å resolution using synchrotron radiation (λ = 0.900 Å). X-ray diffraction data were collected at 100 K and processed to 1.9 Å resolution with 98.2% completeness and an overall $R_{\rm merge}$ of 7.8%. The TcDHOD crystals belong to the orthorhombic space group $P2_12_12_1$, with unit-cell parameters a = 67.87, b = 71.89, c = 123.27 Å. The presence of two molecules in the asymmetric unit (2 × 34 kDa) gives a crystal volume per protein weight ($V_{\rm M}$) of 2.2 Å^3 Da^{-1} and a solvent content of 44%.

1. Introduction

Chagas disease or American trypanosomiasis is caused by the flagellate protozoan parasite *Trypanosoma cruzi* and affects approximately 16–18 million people in Central and South America (World Health Organization, 2001). The progression of this disease can lead to symptoms such as inflammatory cardiomyopathy, digestive injuries and neural disorders. Infection with this protozoan parasite has proven to be extremely difficult to cure, particularly during the chronic phase when most people are diagnosed (Garasia, 2001). A large percentage of Chagas patients receive no specific antiparasitic therapy because of the ineffectiveness and toxicity of existing pharmacologic agents (Estani *et al.*, 1998; Urbina, 2001). Hence, better therapeutic agents are urgently needed.

Dihydroorotate dehydrogenases (DHODs) are flavoenzymes catalyzing the oxidation of L-dihydroorotate to orotate, the fourth step and the only redox reaction in the *de novo* pyrimidine-biosynthesis pathway. On the basis of amino-acid sequence homology DHODs have been classified into two families, referred to as family 1 and family 2. DHODs of family 1 are cytoplasmic enzymes and are further subdivided into families 1A and 1B. The family 1A enzymes are homodimers and appear to utilize fumarate as their physiological oxidant, whereas the family 1B enzymes (heterotetramers) utilize nicotinamide adenine dinucleotide through the intermediary of a second protein subunit containing an Fe_2S_2 cluster and a flavin adenine dinucleotide molecule. Family 2 DHODs, which exist as homodimers or monomers, are membrane-bound enzymes that utilize respiratory quinones as their physiological oxidants (Jensen & Bjornberg, 1998). TcDHOD, belonging to family 1A, exists as a homodimer (MW 2 × 34 kDa) and in addition to DHOD activity also possesses fumarate reductase activity. This suggests that TcDHOD is involved not only in the *de novo* biosynthesis of pyrimidines but also in the redox homeostasis of the parasite (Gao *et al.*, 1999; Nara *et al.*, 2000; Takashima *et al.*, 2002). In contrast, human DHOD belongs to family 2. This great diversity between parasite and host DHODs makes this enzyme a potential target for new chemotherapeutic drugs.

The crystal structures of human DHOD (Liu *et al.*, 2000), *Lactococcus lactis* DHOD A (Rowland *et al.*, 1998) and *Escherichia coli* DHOD (Norager *et al.*, 2002) have been reported. TcDHOD shows a

high level of homology and 55% sequence identity with *L. lactis* DHOD A (Gao *et al.*, 1999). Determination of the structure of TcDHOD should help in the development of new TcDHOD-specific drugs. This should also help to clarify the catalytic mechanism of dihydroorotate oxidation by family 1A DHODs. Here, we report the overexpression, purification, crystallization and preliminary X-ray diffraction studies of TcDHOD complexed with orotate.

2. Materials and methods

2.1. Overexpression of TcDHOD

The gene coding for TcDHOD was cloned by the polymerase chain reaction (PCR). The template for the PCR was the *pyr4* gene (DHOD2; access No. AB122956) from *T. cruzi* present on plasmid pET28a from BL21(DE3)/pET28aTcDHOD (Takashima *et al.*, 2002; Annoura *et al.*, 2005), which expresses His_6-tagged TcDHOD. The primers for the PCR were 5′-CAT ATG ATG TGT CTG AAG CTC-3′ and 5′-CGG GAT CCT CAC TCA ATT GTC TTG AC-3′, which were designed to generate *Bam*HI and *Nde*I sites at the start and the end of the DNA fragment, respectively. The 950 bp PCR product was ligated into the pZErO-2 cloning vector. After transformation of the *E. coli* strain TOP 10 with the ligation mixture, kanamycin-resistant colonies were selected on agar plates. Plasmids were isolated from ten independent colonies and then sequenced. The correct DNA sequence of the cloned PCR fragment in pZErO-2 was further confirmed by DSQ-2000L (Shimadzu) using the Thermo Sequenase fluorescently labelled primer cycle sequencing kit and 7-deaza-dGTP (Amersham Bioscience). The plasmid pZErO-2-TcDHOD was digested with *Bam*HI and *Nde*I and the approximately 950 bp cDNA was inserted into the pET3a expression vector (Novagen). The resulting construct was used for transformation of *E. coli* BL21 (DE3). Single colonies grown on Luria–Bertani (LB) agar containing 100 μg ml^{-1} ampicillin were selected and grown in LB medium containing the same concentration of antibiotic.

The expression of TcDHOD was induced by the addition of 1 m*M* isopropyl β-D-thiogalactopyranoside (IPTG) when the cell culture had attained late log phase (optical density at 550 nm of 0.3). Expression conditions were optimized by examining the effect of the IPTG concentration, temperature and time of induction on the expression levels in total cell lysates as determined by SDS–PAGE and the DHOD activity in soluble protein extracts. The best expression was achieved by induction with 1 m*M* IPTG for 16 h at 298 K.

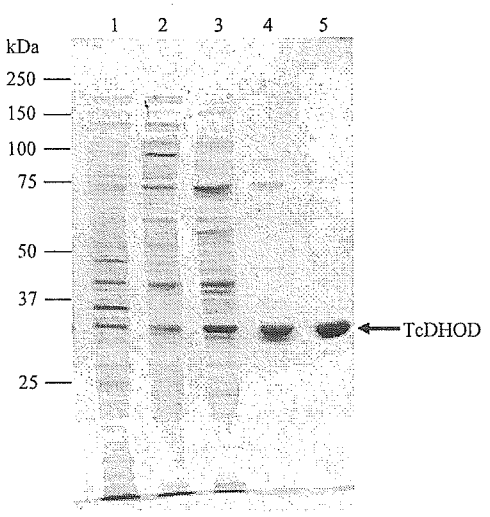

Figure 1
A Coomassie Brilliant Blue-stained 12.5% SDS–PAGE gel showing the purification of TcDHOD. Lane 1, homogenate fraction (5 μg); lane 2, cytoplasmic fraction (5 μg); lanes 3, 4, and 5, pooled fractions after DEAE Sepharose Fast Flow (5 μg), Phenyl Sepharose High Performance (1 μg) and TSK gel G3000SW (1 μg) columns, respectively.

2.2. Purification of recombinant TcDHOD

All purification steps were conducted at 277 K. The cells were harvested from 10 l of culture by centrifugation for 10 min at 1700*g*. After three washes in 50 m*M* Tris–HCl pH 8.0 containing 3 m*M* ethylenediaminetetraacetic acid (EDTA) and 0.1 m*M* phenylmethylsulfonyl fluoride, the yellow pellet was resuspended in lysis buffer (50 m*M* Tris–HCl pH 8.0, 20 m*M* EDTA, 0.25 m*M* sodium orotate). After addition of hen egg-white lysozyme to a final concentration of 2 mg ml^{-1}, the mixture was stirred for 10 min. The lysate was then homogenized in a Waring blender to reduce its viscosity and the cells were broken with a French press at 130 MPa. The inclusion-body fraction was removed by centrifugation at 26 000*g* for 15 min. Streptomycin sulfate was added to the yellow supernatant to a final concentration of 1%(*w*/*v*). The solution was stirred for 30 min and the precipitate, primarily consisting of nucleic acids, was removed by centrifugation for 30 min at 26 000*g*. The soluble protein extract was obtained as a supernatant following centrifugation at 200 000*g* for 1.5 h.

The soluble protein extract was filtered through a 0.22 μm pore-size filter and applied onto a DEAE Sepharose Fast Flow (Amersham Bioscience) column (5.0 × 30 cm) pre-equilibrated in 10 m*M* Tris–HCl pH 8.0 containing 0.25 m*M* sodium orotate. The column was washed with 2.5 l of the same buffer and then eluted with a 5 l gradient of 0.0–0.5 *M* NaCl at a flow rate of 10 ml min^{-1}. The yellow fractions containing TcDHOD, which eluted at 0.25–0.3 *M* NaCl, were pooled. Ammonium sulfate, sodium orotate and sodium phosphate buffer pH 7.5 were added to final concentrations of 1.2 *M*, 0.25 m*M* and 50 m*M*, respectively. After stirring for 30 min, the supernatant following centrifugation for 30 min at 26 000*g* was loaded onto a Phenyl Sepharose High Performance (Amersham Bioscience) column (1.6 × 60 cm) pre-equilibrated with 50 m*M* sodium phosphate buffer pH 7.5 containing 1.2 *M* ammonium sulfate and 0.25 m*M* sodium orotate. After washing with 600 ml of the same buffer, TcDHOD was eluted with a 1.5 l gradient of 1.2–0.0 *M* ammonium sulfate at a flow rate of 5 ml min^{-1}. The active peak fractions were pooled and the buffer was changed to 100 m*M* sodium phosphate buffer pH 7.5 containing 0.25 m*M* sodium orotate by repeated dilution and concentration with a Vivaspin centrifugal concentrator tube (Vivaspin 20, 10K MWCO). The concentrated enzyme solution (25–30 mg ml^{-1}) was applied onto a TSK G3000SW (Tosoh) gel-filtration column (7.5 × 600 mm) and the column was run at a flow rate of 1 ml min^{-1}. The active fractions were pooled and concentrated with a Vivaspin 20 (10K MWCO) to 40 mg ml^{-1}. Glycerol was added to a final concentration of 50%(*v*/*v*) and the purified protein was stored in small aliquots at 243 K until use. The DHOD activity was assayed as described previously (Takashima *et al.*, 2002). TcDHOD was purified to apparent homogeneity as shown by SDS–PAGE (Fig. 1) and was purified 40-fold compared with the cytoplasmic fraction, with a recovery of 10–15 mg from 10 l of culture. Sodium orotate was added to all of the purification steps to stabilize the enzyme activity.

2.3. Crystallization and X-ray data collection

Crystallization was performed by the sitting-drop vapour-diffusion technique using 96-well CrystalClear Strips (Hampton Research). The experiments were carried out by mixing 1 µl protein solution (10 mg ml^{-1} in 10 m*M* Tris–HCl pH 8.0 containing 1 m*M* orotate) with an equal volume of reservoir solution and allowing the drop to equilibrate with 150 µl reservoir solution. Initial crystallization conditions for TcDHOD were screened at 277 and 293 K using Crystal Screen (Jancarik & Kim, 1991) and Crystal Screen II (Hampton Research) and Wizard Screens I and II (Emerald BioStructures). Out of 194 conditions, only No. 27 from Wizard Screen II [10%(*w*/*v*) PEG 3000, 0.1 *M* cacodylate pH 6.5 and 0.2 *M* $MgCl_2$] gave crystals at 277 K. However, these were aggregates of tiny needle-shaped crystals that were not suitable for X-ray diffraction experiments. The crystallization conditions were then optimized using PEGs with different molecular weights and by varying the PEG concentration, the pH and the temperature, but none of the conditions resulted in a marked improvement.

We next tried PEG/Ion Screen and Additive Screen kits (Hampton Research) to examine the effect of adding various salts and additives. Plate-shaped orange–brown single crystals appeared when sodium thiocyanate and hexaamminecobalt (III) chloride were used as additives. The best crystals grew at 277 K from 16%(*w*/*v*) PEG 3350 as the main precipitating agent in 100 m*M* cacodylate pH 6.2, 1 m*M* sodium orotate, 50 m*M* hexaamminecobalt (III) chloride and 1 m*M* sodium thiocyanate. The addition of 50 m*M* hexaamminecobalt (III) chloride and 1 m*M* sodium thiocyanate caused no detectable change in the enzymatic activity of TcDHOD, indicating that the effects of these reagents are only on crystallization.

Diffraction data were collected under liquid-nitrogen-cooled conditions at 100 K. A crystal mounted in a nylon loop was transferred and soaked briefly in reservoir solution supplemented with 20%(*v*/*v*) glycerol and then frozen by rapidly submerging it in liquid nitrogen. X-ray diffraction data were collected by the rotation method at the BL44XU beamline of SPring-8 using a DIP6040 detector at a wavelength of 0.900 Å. A total of 180 frames were recorded with an oscillation angle of 1°, an exposure time of 5 s per frame and a crystal-to-detector distance of 250 mm. The intensities were integrated with *MOSFLM* (Leslie, 1992) and scaled with *SCALA* (Evans, 1993) from the *CCP*4 suite (Collaborative Computational Project, Number 4, 1994).

Table 1
Statistics of data collection and processing.

Values for the highest resolution shell are given in parentheses.

Wavelength (Å)	0.900
Space group	$P2_12_12_1$
Unit-cell parameters (Å)	a = 67.87, b = 71.89, c = 123.27
Resolution range (Å)	28.3–1.9 (2.0–1.9)
No. of reflections	196908
Unique reflections	47235
Completeness (%)	98.2 (99.4)
R_{merge} (%)	7.8 (20.1)
$I/\sigma(I)$	6.5 (3.2)

3. Results and discussion

The first crystallization trials of TcDHOD were carried out using His_6-tagged TcDHOD, but we were unable to obtain crystals. As found when expressing the recombinant SH3 domain of chicken tyrosine kinase in *E. coli* (Kim *et al.*, 2001), this problem can occur owing to spontaneous α-*N*-6-phosphogluconoylation at the His_6 tag site even if SDS–PAGE and dynamic light scattering show the protein to be homogeneous (Geoghegan *et al.*, 1999). For this reason, we removed the His_6 tag from His_6-TcDHOD using thrombin, but this resulted in complete loss of enzymatic activity. As a final attempt, we used an alternative expression system to produce native TcDHOD without the His_6 tag. Although the expressed enzyme gradually lost its enzymatic activity during purification, the addition of 0.25 m*M* sodium orotate stabilized the enzyme for more than several weeks. The enzyme could be purified to homogeneity (>95%) using sequential steps of ion-exchange, hydrophobic interaction and gel-filtration chromatography.

The best crystals were obtained at 277 K in the presence of 16%(*w*/*v*) PEG 3350, 100 m*M* cacodylate pH 6.2, 1 m*M* sodium orotate, 50 m*M* hexaamminecobalt (III) chloride and 1 m*M* sodium thiocyanate. The crystals usually appeared within 1 d and reached maximum dimensions of 0.15 × 0.10 × 0.03 mm after a week (Fig. 2). The crystals are stable and can be kept for several months. Although significant reflections were observed beyond 1.8 Å resolution at the beginning of data collection, radiation damage gradually diminished the reflections at higher resolution. A good-quality data set to 1.9 Å resolution was obtained after scaling and merging the 180 images. The data-collection and processing statistics are summarized in Table 1.

Analysis of the symmetry and systematic absences in the recorded diffraction pattern indicates that the crystals belong to the orthorhombic space group $P2_12_12_1$, with unit-cell parameters a = 67.87, b = 71.89, c = 123.27 Å. Assuming the presence of two TcDHOD molecules in the asymmetric unit, the calculated Matthews coefficient (Matthews, 1968) is 2.2 Å^3 Da^{-1}, which corresponds to a solvent content of 44%. An attempt to solve the structure using molecular replacement with the *MOLREP* program (Navaza, 1994) as implemented within the *CCP*4 package (Collaborative Computational Project, Number 4, 1994) was carried out using the refined coordinates of DHOD A from *L. lactis* (PDB code 1ovd), with which TcDHOD shows 55% sequence identity. X-ray diffraction data in the resolution range 8.0–4.0 Å were used. The best solution had a correlation coefficient (CC) of 0.654 and an R factor of 51.4%, while for the second-best solution the CC was 0.412 and the R factor was 58.0%. The model subsequently subjected to rigid-body refinement gave an R factor of 45.5% and further refinement of the dimer structure of TcDHOD complexed with orotate is in progress. The current R factor is 21.5% (R_{free} = 25.5%) and the electron-density map clearly shows the orotate molecule as stacking with the FMN. In

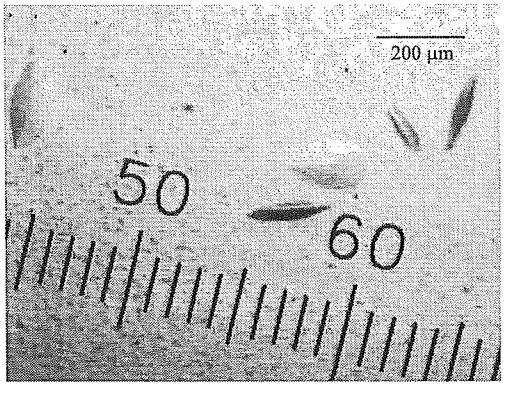

Figure 2
Crystals of *T. cruzi* dihydroorotate dehydrogenase obtained by sitting-drop vapour diffusion in the presence of 16%(*w*/*v*) PEG 3350 with 50 m*M* hexaamminecobalt (III) chloride as an additive.

parallel with the refinement, we are also trying to obtain crystals of TcDHOD complexed with a variety of other ligands, such as substrate analogues and effector-site inhibitors.

Since TcDHOD is essential for the survival and growth of *T. cruzi* (Annoura *et al.*, 2005), this enzyme is a promising target for chemotherapy. It is hoped that the details of the interactions between TcDHOD and ligands will help elucidate the catalytic mechanism of TcDHOD and advance structure-based drug design aimed at Chagas disease.

References

Annoura, T., Nara, T., Makiuchi, T., Hashimoto, T. & Aoki, T. (2005). *J. Mol. Evol.* **60**, 113–127.

Collaborative Computational Project, Number 4 (1994). *Acta Cryst.* D**50**, 760–763.

Estani, S. S., Segura, E. L., Ruiz, A. M., Valazquez, E., Porcel, B. M. & Yampotis, C. (1998). *Am. J. Trop. Med. Hyg.* **55**, 586–588.

Evans, P. R. (1993). *Proceedings of the CCP4 Study Weekend. Data Collection and Processing*, edited by L. Sawyer, N. Isaacs & S. Bailey, pp. 114–122. Warrington: Daresbury Laboratory.

Gao, G., Nara, T., Nakajima-Shimada, J. & Aoki, T. (1999). *J. Mol. Biol.* **285**, 149–161.

Garasia, L. S. (2001). *Diagnostic Medical Parasitology*, 4th ed. Washington, DC: ASM Press.

Geoghegan, K. F., Dixon, H. B. F., Rosner, P. J., Hoth, L. R., Lanzetti, A. J., Borzilleri, K. A., Marr, E. S., Pezzulo, L. H., Martin, L. B., Lemotte, P. K., McColl, A. S., Kamath, A. V. & Stroh, J. G. (1999). *Anal. Biochem.* **267**, 169–184.

Jancarik, J. & Kim, S.-H. (1991). *J. Appl. Cryst.* **24**, 409–411.

Jensen, K. F. & Bjornberg, O. (1998). *Paths Pyrimidines*, **6**, 20–28.

Kim, K. M., Yi, E. C., Baker, D. & Zhang, K. Y. J. (2001). *Acta Cryst.* D**57**, 759–762.

Leslie, A. G. W. (1992). *Jnt CCP4/ESF–EACBM Newsl. Protein Crystallogr.* **26**.

Liu, S., Neidhardt, E. A., Grossman, T. H., Ocain, T. & Clardy, J. (2000). *Structure Fold. Des.* **8**, 25–33.

Matthews, B. W. (1968). *J. Mol. Biol.* **33**, 491–497.

Nara, T., Hashimoto, T. & Aoki, T. (2000). *Gene*, **256**, 209–222.

Navaza, J. (1994). *Acta Cryst.* A**50**, 157–163.

Norager, S., Jensen, K. F., Bjornberg, O. & Larsen, S. (2002). *Structure*, **10**, 1211–1223.

Rowland, P., Bjornberg, O., Nielsen, F. S., Jensen, K. F. & Larsen, S. (1998). *Protein Sci.* **7**, 1269–1279.

Takashima, E., Inaoka, D. K., Osanai, A., Nara, T., Odaka, M., Aoki, T., Inaka, K., Harada, S. & Kita, K. (2002). *Mol. Biochem. Parasitol.* **122**, 189–200.

Urbina, J. A. (2001). *Curr. Opin. Infect. Dis.* **6**, 733–741.

World Health Organization (2001). *Chagas.* http://www.who.int/ctd/chagas/disease.htm.

Available online at www.sciencedirect.com
SCIENCE DIRECT®
Biochemical and Biophysical Research Communications 334 (2005) 593–600
BBRC
www.elsevier.com/locate/ybbrc

Mutational analysis of the *Trypanosoma vivax* alternative oxidase: The $E(X)_6Y$ motif is conserved in both mitochondrial alternative oxidase and plastid terminal oxidase and is indispensable for enzyme activity ☆,☆☆

Kosuke Nakamura [a], Kimitoshi Sakamoto [a], Yasutoshi Kido [a], Yoko Fujimoto [a], Takashi Suzuki [b], Mitsuko Suzuki [b], Yoshisada Yabu [b], Nobuo Ohta [b], Akiko Tsuda [c], Misao Onuma [c], Kiyoshi Kita [a,*]

[a] *Department of Biomedical Chemistry, Graduate School of Medicine, The University of Tokyo, Tokyo 113-0033, Japan*
[b] *Department of Molecular Parasitology, Nagoya City University, Graduate School of Medical Sciences, Nagoya 467-8601, Japan*
[c] *Graduate School of Veterinary Medicine, Hokkaido University, Sapporo 060-0818, Japan*

Received 20 June 2005
Available online 1 July 2005

Abstract

Based on amino acid sequence similarity and the ability to catalyze the four-electron reduction of oxygen to water using a quinol substrate, mitochondrial alternative oxidase (AOX) and plastid terminal oxidase (PTOX) appear to be two closely related members of the membrane-bound diiron carboxylate group of proteins. In the current studies, we took advantage of the high activity of *Trypanosoma vivax* AOX (TvAOX) to examine the importance of the conserved Glu and the Tyr residues around the predicted third helix region of AOXs and PTOXs. We first compared the amino acid sequences of TvAOX with AOXs and PTOXs from various taxa and then performed alanine-scanning mutagenesis of TvAOX between amino acids Y_{199} and Y_{247}. We found that the ubiquinol oxidase activity of TvAOX is completely lost in the E214A mutant, whereas mutants E215A and E216A retained more than 30% of the wild-type activity. Among the Tyr mutants, a complete loss of activity was also observed for the Y221A mutant, whereas the activities were equivalent to wild-type for the Y199A, Y212A, and Y247A mutants. Finally, residues Glu_{214} and Tyr_{221} were found to be strictly conserved among AOXs and PTOXs. Based on these findings, it appears that AOXs and PTOXs are a novel subclass of diiron carboxylate proteins that require the conserved motif $E(X)_6Y$ for enzyme activity.

Keywords: Trypanosome alternative oxidase; Ascofuranone; Diiron carboxylate proteins; Diiron binding motif; *Escherichia coli* expression; Mutagenesis

The alternative oxidase (AOX) has been found in the Plantae, Fungi, Protita, and Eubacteria kingdoms. Recent genome database searches have also revealed the presence of AOX in different phyla of the Animalia kingdom, including Mollusca, Nematoda, and Chordata [1]. The ubiquitous presence of the AOX suggests that it has a general physiological role, including maintenance of the cellular redox balance and protection against oxidative stress [2]. Like heme-containing terminal

☆ New nucleotide sequence reported in this paper is available in the DDBJ, EMBL, and NCBI databases under the Accession No. AB211244.

☆☆ *Abbreviations:* ALA, 5-aminoleuvulic acid; AOX, alternative oxidase; AF, ascofuranone; DMSO, dimethylsulfoxide; IPTG, isopropropyl-β-D-thiogalactopyranoside; PTOX, plastid terminal oxidase; SHAM, salicylhydroxamic acid; TAO, trypanosome alternative oxidase; TvAOX, *Trypanosoma vivax* alternative oxidase; Y/Tyr, tyrosine; E/Glu, glutamate; OD_{600nm}, optical density of light of wavelength 600 nm.

* Corresponding author. Fax: +81 3 5841 3444.
E-mail address: kitak@m.u-tokyo.ac.jp (K. Kita).

0006-291X/$ - see front matter © 2005 Elsevier Inc. All rights reserved.
doi:10.1016/j.bbrc.2005.06.131

oxidases, such as cytochrome *c* oxidase in the respiratory chain, AOX catalyzes the four-electron reduction of oxygen to form water. Because the electron flow does not couple with proton translocation, AOX represents a non-energy conservation branch of electron transport, bypassing the last two sites of proton translocation (complexs III and IV) associated with the cytochrome pathway [3]. Spectroscopic studies of the partially purified enzyme indicate that AOXs are also distinct because they do not contain a heme or an iron–sulfur center [2]. The AOX is therefore cyanide-resistant, although inhibitors have been reported, including salicylhydroxamic acid (SHAM), propyl gallate, and ascofuranone (AF), which is the most potent inhibitor of AOX [4–6]. Studies in *Pichia anomala* AOX [7] and *Trypanosoma brucei brucei* AOX [8] show that, despite the lack of a heme or an iron–sulfur center, the enzyme requires iron for activity. The binding of iron by AOXs may be mediated by four sequence motifs, namely two –E– and two –EXXH– sequences, which are known to be the binuclear iron-binding motifs in ribonucleotide reductase R2, methane monooxygenase, and Δ9-desaturase [9].

The plastid terminal oxidase (PTOX) was discovered by analysis of the *Immutans* (*imm* mutant) of *Arabidopsis thaliana*, which is defective in chloroplast biogenesis and is localized at the thylakoid membrane of the plastid [1,10,11]. Based on sequence similarity, including the binuclear iron binding sequences, AOX and the PTOX are members of the membrane-bound diiron carboxylate group of proteins. Moreover, their similarity is highlighted by the fact that they both carry out four-electron reduction of oxygen to water using quinol as an electron donor [12,13]. According to a recent structural model by Andersson and Nordlund [14], the hydrophobic regions in AOX are not membrane spanning as originally proposed but rather interfacial. Because of the sequence and functional similarity to AOX, PTOX is predicted to be an interfacial membrane protein with a diiron center in the active site [15].

The identification of one of the binuclear iron binding sequences (–E–) in the third helix of the AOXs by enzymatic analysis has been controversial because the triplet Glu region (LEEEA) is highly conserved in AOXs [3,8,16]. In addition, it was suggested that analysis of this region would be difficult because any alteration in this region could hinder substrate binding and/or accessibility to the active site [8] or reduce the structural stability of the active site [3]. Of the three Glu residues in this motif, only the first is strictly conserved among both the AOXs and the PTOXs. However, the essential role of this first Glu residue has not yet been proven, whereas the importance of the second and third has been demonstrated by mutational analysis [3,16]. In addition to Glu residues, Tyr has been suggested to be involved in radical formation during electron transfer as well as in quinone binding [9]. Four Tyr residues, two in the third helix and two near the helix, are also strictly conserved in the AOXs.

Here, we investigated the importance of Glu and Tyr residues in the function of AOXs by alanine-scanning mutagenesis of all Glu and Tyr residues around the predicted third helix (Y_{199}-ITSPRFVHRFVGYLEEEA VVTYTGILRAIDDGRLPPMKNAVPDVARV-Y_{247}). We took advantage of the high quinol oxidase activity of TvAOX to characterize the role of these residues in the activity of AOXs and PTOXs. Based on the conservation of Glu and Tyr residues and their role in the activity of TvAOX, we showed the first direct evidence that the motif, $E(X)_6Y$, is essential for the activity of AOXs and PTOXs. This suggests that AOXs and PTOXs are a novel subclass of diiron carboxylate proteins that share the $E(X)_6Y$ motif.

Materials and methods

Chemicals. All chemicals were of biochemical grade. Ubiquinone-1,5-aminolevulinic acid (ALA), kanamycin, carbenicillin, and protease inhibitor cocktail were obtained from Sigma–Aldrich Japan (Tokyo, Japan). Isopropropyl-β-D-thiogalactopyranoside (IPTG) was obtained from Wako Pure Chemical Industries (Tokyo, Japan). Dimethyl sulfoxide (DMSO) was from Nacalai Tesque (Kyoto, Japan). Ascofuranone (AF) was isolated from *Ascochyta visiae* and handled as previously described [17]. The stock solution of AF was prepared in DMSO at 100 mM and stored at −20 °C. Before use, it was diluted with ethanol to the required concentration.

Sequence alignment. The complete amino acid sequences for AOX and PTOX from a variety of organisms were aligned using the Clustal W, version 1.81 [18] with default gap penalties. The aligned sequences were then rearranged for presentation using BOXSHADE, version 3.21 (available at URL:http://www.ch.embnet.org/software/BOX_form.html). GenBank Accession Nos. of the sequences are as follows: *Trypanosoma vivax AOX* (AB070521), *Trypanosoma brucei brucei* AOX (AB070614), *Trypanosoma brucei rhodesiense* AOX (AB211244), *Cryptosporidium hominis* AOX (EAL35765), *Cryptosporidium parvum* AOX (AB118216), *Neurospora crassa* AOX (L46869), *Sauromatum guttatum* AOX (AAA34048), *Glycine max* AOX (U87906), *Arabidopsis thaliana* PTOX (AF098072), *Oryza sativa* PTOX (AAC35554), *Prochlorococcus marinus* PTOX (CAE18795), and *Synechococcus* sp. PTOX (NP_896980).

Construction of Escherichia coli transformants with vectors for expression of mutated TvAOX. In these studies, we used the expression vector pTvAOX, which carries a cDNA fragment containing the whole TvAOX coding region with *Nde*I (5′-end) and *Bam*HI sites (3′-end) in the pET15b expression vector (Novagen, La Jolla, CA) [6]. Mutations were introduced using the QuickChange Site-directed Mutagenesis Kit (Stratagene Cloning Systems, La Jolla, CA) according to the manufacturer's instructions. Oligonucleotides specific to each mutation are shown in Table 1, with altered codons indicated in bold and italics. *E. coli* DH5α was used for cloning, and transformants were plated on Luria–Bertani (LB) plates containing carbenicillin (100 μg/mL) and incubated overnight at 37 °C. Plasmid DNAs were obtained from a single colony by the alkali method as previously described [5]. *E. coli/hemA* mutant strain *E. coli*/Δ*hemA* cells (F^- *ompT* $hsdS_B(r_B^-m_B^-)$ *gal dcm* (DE3)Δ*hemA*::Km^r) [5] were then transformed with each of the specifically mutated TvAOX expression vectors. The cloned cells were stored in 10% (w/v) glycerol at −80 °C until use.

Preparation of recombinant TvAOX. The resulting stable *E. coli*/Δ*hemeA* transformants were grown for 10 h on LB plates supplemented

Table 1
Mutagenic oligonucleotides used to construct site-directed TvAoX mutants

Strain	TAO version	Mutated residue[a]	Mutation primer sequence[b]
pET 15b	None	None	None
WT	TvAOX	None	None
E214A	TvAOX (E214A)	$Glu_{214} \rightarrow$ Ala	5′-CGTTTTGTGGGTTAACCTT***GCG***GAAGAAGCTGTTGTGAC-3′ 5′-GTCACAACAGCTTCTTC***CGC***AAGGTAACCCACAAAACG-3′
E215A	TvAOX (E215A)	$Glu_{215} \rightarrow$ Ala	5′-CGTTTTGTGGGTTACCTTGAG***GCA***GAAGCTGTTGTGAC-3′ 5′-GTCACAACAGCTTC***TGC***CTCAAGGTAACCCACAAAACG-3′
E216A	TvAOX (E216A)	$Glu_{216} \rightarrow$ Ala	5′-GGGTTACCTTGAGGAA***GCA***GCTGTTGTGACATACAC-3′ 5′-GTGTATGTCACAACAGC***TGC***TTCCTCAAGGTAACCC-3′
Y247A	TvAOX (Y247A)	$Tyr_{247} \rightarrow$ Ala	5′-TGATGTGGCAAGGGTG***GCC***TGGGGCCTCAACAA-3′ 5′-TTGTTGAGGCCCCA***GGC***CACCCTTGCCACATCA-3′
Y221A	TvAOX (Y221A)	$Tyr_{221} \rightarrow$ Ala	5′-GAAGAAGCTGTTGTGACA***GCC***ACTGGTATCCTGCGCGCC-3′ 5′-GGCGCGCAGGATACCAGT***GGC***TGTCACAACAGCTTCTTC-3′
Y212A	TvAOX (Y212A)	$Tyr_{212} \rightarrow$ Ala	5′-GTGCATCGTTTTGTGGGT***GCC***CTTGAGGAAGAAGCTG-5′ 5′-CAGCTTCTTCCTCAAG***GGC***ACCCACAAAACGATGCAC-3′
Y199A	TvAOX (Y199A)	$Tyr_{199} \rightarrow$ Ala	5′-GCTTCCTTCTTATTGCT***GCC***ATTACCTCGCCGCGCTTC-3′ 5′-GAAGCGCGGCGAGGTAAT***GGC***AGCAATAAGAAGGAAGC-3′

[a] Residue and nucleotide positions are those relative to the translation start site of TvAOX reported previously by Suzuki et al. [4].
[b] Codons which contain site-directed mutations are in bold italics.

with ALA (100 μg/mL), carbenicillin (100 μg/mL), and kanamycin (50 μg/mL), after which a single colony was picked and used to inoculate 5 mL of the small culture liquid S-medium (5 g/L casamino acids, 0.05 g/L magnesium sulfate, 10.4 g/L dipotassium hydrophosphate, 3 g/L potassium dihydrogen phosphate, 0.75 g/L sodium citrate, 2.5 g/L ammonium sulfate, 10 g/L tryptone peptone, 5 g/L yeast extract, 25 mg/L iron sulfate, and 25 mg/L iron chloride) with ALA (100 μg/mL) at 30 °C. After a 4-h incubation, the cells were washed with fresh sterilized culture medium without ALA. This cell suspension was used to inoculate 100 ml of S-medium containing carbenicillin (100 μg/mL) and kanamycin (50 μg/mL) to $OD_{600nm} = 0.01$. The cells were then grown at 30 °C with continuous shaking (150 rpm; BR40LF shaker, TITEC, Tokyo, Japan) to $OD_{600nm} = 0.1$. The recombinant protein was then induced by addition of 25 μM IPTG. The bacterial growth was continuously monitored at OD_{600nm} by a UV-1200 UV–Vis spectrophotometer (Shimadzu, Kyoto, Japan). After 4.5 h of induction, cells were harvested by centrifugation at 4 °C, resuspended in 50 mM Tris–HCl (pH 7.5) containing protease inhibitor cocktail 4-(2-aminoethyl)benzenesulfonyl fluoride (AEBSF), ethylene diamine tetra-acetic acid (EDTA), bestatin, E-64, leupeptin, and aprotinin at the concentrations recommended by the manufacturer, sonicated five times for 10 s in a 2.2-mL polypropylene tube on ice with an automated Sonifier S-450A (Branson, Danbury, CT), and centrifuged at 12,000*g* for 15 min at 4 °C. The supernatant was further separated into cytoplasm and membrane fractions by ultracentrifugation in a CS100FX centrifuge (Hitachi, Ibaraki, Japan) at 200,000*g* for 1 h at 4 °C. The resulting pellet was resuspended in 50 mM Tris–HCl (pH 7.5) containing protease inhibitor cocktail and used as the membrane fraction.

Ubiquinol oxidase assay. The assay of ubiquinol oxidase activity was based on a previously described protocol [5]. Briefly, the absorbance change of ubiquinol-1 at 278 nm was monitored using a UV-3000 spectrophotometer (Shimadzu). A 995-μL mixture of membrane fraction in 50 mM Tris–HCl (pH 7.5) was preincubated for 3 min at 25 °C and then mixed with 5 μL of 150 μM ubiquinol-1 (molar extinction coefficient = 15,000) in ethanol to initiate the reaction. To assay the ability of AF to inhibit the enzyme activity, AF diluted in ethanol was added to the reaction mixture prior to the addition of ubiquinol-1. All conditions were assayed at least six times. The results are representative of four independent experiments.

Gel electrophoresis and Western blotting. Proteins were separated by electrophoresis on sodium dodecyl sulfate (SDS)–polyacrylamide gels as described previously [6]. The separated proteins were transferred to polyvinylidene fluoride (PVDF) membranes and detected by Western blotting with monoclonal antibody WM-211 [6].

Statistical analysis. All data were presented as means ± standard deviation and tested by one-way analysis of variance (ANOVA). The data were subsequently subjected to Tukey's test to determine significance of differences among mutants. Differences were considered significant at $p < 0.05$.

Results and discussion

The sequence comparison of AOX and PTOX based on the protein model

Fig. 1A shows the amino acid sequence alignment of seven AOXs and four PTOXs from a variety of taxa. It should be noted that the nucleotide sequence of *T. b. rhodesiense* was completely identical to that of the *T. b. brucei* [19]. The recent structural model of AOX and PTOX proposes that, similar to other diiron carboxylate proteins, both enzymes are folded on the surface of the membrane and form a diiron center within four helices [14]. Only a limited number of residues were completely conserved in the four predicted helices, and they are indicated in the figure with asterisks below the sequences. Arrowheads above the sequences indicate the highly conserved Glu and His residues that are known to constitute the diiron-binding motifs and are positioned in each of the three predicted α-helices in the model [14]. Fig. 1B shows all Glu and Tyr residues around the third helix of TvAOX. There are three Glu

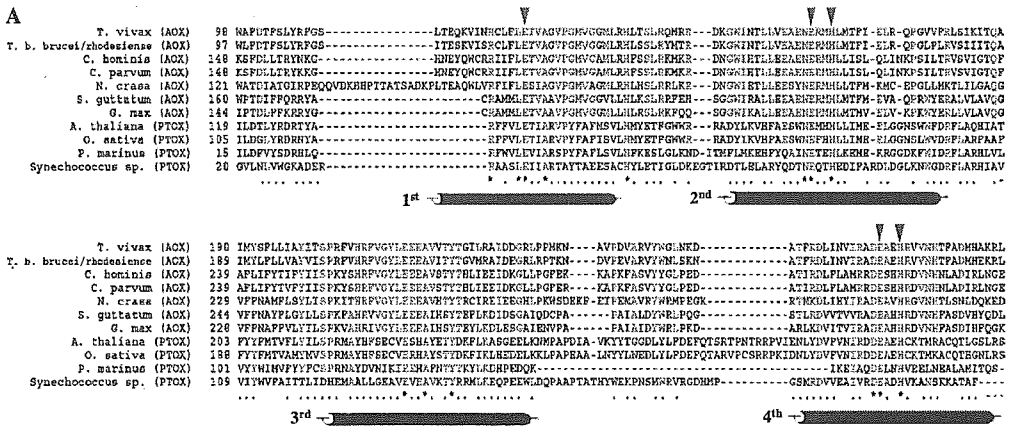

B

		6 amino acids					
***T. vivax* AOX**	Y	Y	E	E	E	Y	Y
	199	212	214	215	216	221	247
***T. b. brucei / rhodesiense* AOX**	198	211	213	214	215	220	246
***C. hominis* AOX**	248	261	263	264	265	270	296
***C. parvum* AOX**	248	261	263	264	265	270	296
***N. crasa* AOX**	238	251	253	254	255	260	289
***S. guttatum* AOX**	253	266	268	269	270	275	299
***G. max* AOX**	237	250	252	253	254	259	283
***A. thaliana* PTOX**	212	N/A	227	N/A	N/A	234	N/A
***O. sativa* PTOX**	197	N/A	212	N/A	N/A	219	N/A
***P. marius* PTOX**	110	N/A	125	126	N/A	132	N/A
***Synechococcus sp.* PTOX**	N/A	N/A	133	N/A	135	140	N/A

Fig. 1. (A) Sequence alignment of AOX and PTOX proteins from various prokaryotic and eukaryotic taxa using Clustal W program, version 1.81 with default gap penalties. Residues in red are identical, and residues in blue have similar characteristics. The bars below the sequences indicated the predicted helices according to the Andersson and Nordlund model [14]. Arrowheads above the sequences indicated the highly conserved Glu and His residues. (B) All Glu and Tyr residues were analyzed around the third helix of TvAOX, and the corresponding amino acid numbers for the other AOXs and PTOXs are indicated. The alignment of 50 AOXs and 10 PTOXs identified highly conserved Glu and Tyr residues separated by seven amino acids. N/A indicates that the position of the amino acid is not applicable to the corresponding organism.

residues (E_{214}, E_{215}, and E_{216}) in the predicted third helix of the TvAOX that are suspected to contribute to the diiron binding motif. There are also two Tyr residues (Y_{199} and Y_{247}) near the helix and two Tyr residues (Y_{212} and Y_{221}) within the helix. The amino acid numbers corresponding to the residues for the other AOXs and PTOXs are also shown. Only E_{214} and Y_{221} are strictly conserved in this helix region.

Effect of the expression of mutated TvAOX in the E. coli/ΔhemA strain

We next subjected all Glu and Tyr residues around the predicted third helices (Y_{199} toY_{247}) to alanine-scanning mutagenesis to determine which are indispensable for enzyme function. Table 1 shows the oligonucleotide primers used for site-directed mutagenesis of the TvAOX gene. Whole cDNA sequencing confirmed the presence of the targeted mutations and the absence of any other non-specific mutations. The growth of the *E. coli/ΔhemA* strains expressing the recombinant TvAOXs was examined on LB plates at 37 °C (Fig. 2). The *hemA* gene was deleted in the *E. coli/ΔhemA* strain, which prevents it from producing functional cytochrome *bo* and *bd* complexes because they both require heme for the enzyme reaction [5]. Consequently, the respiratory chain of this strain lacks the functional major terminal oxidases. Thus, respiration can be only rescued by providing ALA, a precur-

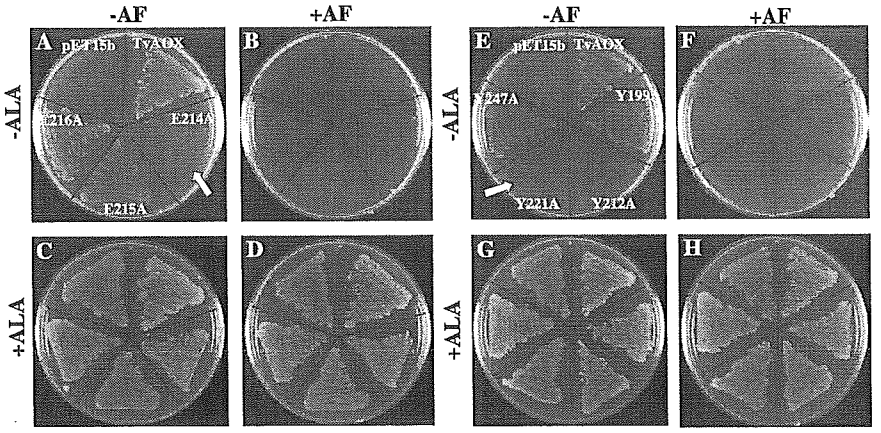

Fig. 2. Effect of the expression of wild-type and mutated TvAOX on the growth of the *E. coli*/Δ*hemA* strain. The control strain carrying an empty vector (pET15b) and strains carrying wild-type or Glu- or Tyr-mutated TvAOXs were cultured on LB plates at 37 °C. All plates were supplemented with 100 μM carbenicillin and 50 μM kanamycin. Plates were neither supplemented with glucose nor IPTG. (B,D,F,H) AF dissolved in DMSO was added to the culture plates at a concentration of 20 μM. Other plates received the same volume of DMSO. The culture plates were supplemented with (C,D,G,H) and without (A,B,E,F) 100 μM ALA. The arrow indicates the strains that showed no apparent growth in the absence of ALA and AF.

sor for heme downstream of the hemA enzyme reaction (Figs. 2C, D, G, and H), or by producing active recombinant TvAOX (Figs. 2A and E). As shown in Figs. 2A and E, all of the recombinant proteins, except for E214A and Y221A, supported the growth of the *E. coli*/Δ*hemA* strain in the absence of ALA. This suggests that the growth defect observed for the E214A and Y221A mutants is due to a loss of TvAOX enzymatic activity.

AOX is resistant to cyanide but is sensitive to a number of other inhibitors. Of these, AF is the most potent [6]. In vitro analysis of enzyme inhibition has revealed that the concentration of AF needed for half-maximal inhibition of recombinant TvAOX is 0.40 nM [6]. This is much more potent than other inhibitors of AOX. For example, AOXs from other species are inhibited by SHAM at 40–260 μM and by propyl gallate at 0.4–4 μM [9]. Because AF specifically inhibits TvAOX at a very low concentration, the presence of TvAOX activity can be directly observed in *E. coli* expression experiments by adding it to the growth media. Figs. 2B and F show that when AF was added to the plate, colony growth was prevented. Thus, in the absence of added ALA, cell growth was highly dependent on the presence of active recombinant TvAOX.

The expression of recombinant protein was checked by electrophoresis followed by staining with Coomassie brilliant blue as well as by Western blotting with a monoclonal antibody specific to the sequences between Asp_{266} and Asn_{274} of TvAOX [6]. As shown in Fig. 3, mutant proteins were expressed and detected as a single band at around 35 kDa in the *E. coli*/Δ*hemA* strain. The Glu (Fig. 3A) or the Tyr (Fig. 3B) to Ala mutations, including E214A and Y221A, did not alter the expression or stability of the protein in this system.

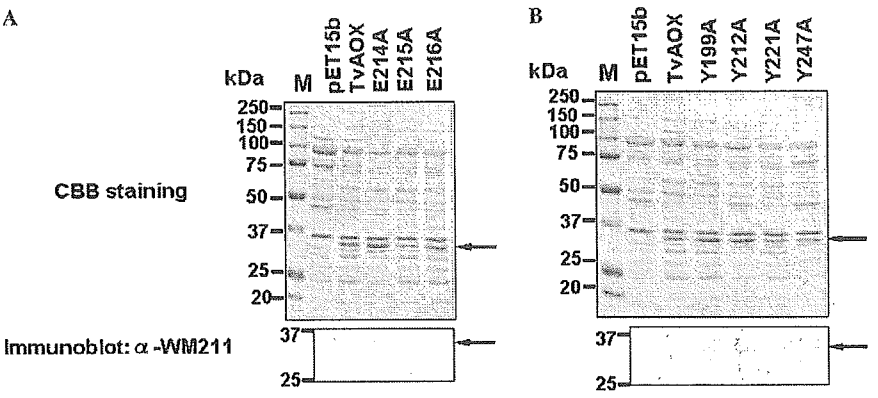

Fig. 3. SDS–polyacrylamide gel electrophoresis and Western blot analysis of the membrane isolates from *E. coli*/Δ*hemA* carrying the empty expression vector (pET15b) or vectors containing the wild-type or mutated TvAOX. Equal amounts of membrane protein (20 μg) were loaded onto a 10% SDS-polyacrylamide gel. Similar to wild-type, staining with Coomassie brilliant blue (above) and Western blotting (below) showed that (A) Glu- and (B) Tyr-mutated TvAOXs were detected at 35 kDa (indicated by the horizontal arrows).

Ubiquinol oxidase activity of the recombinant TvAOXs

In previous mutational analyses, AOX activity was assayed by an indirect method using either NADH or succinate as a substrate for respiratory activity [3,8,9]. Our recombinant system, in contrast, eliminates interference by other quinol oxidizing enzymes so that ubiquinol oxidase activity of TvAOX can be measured directly. This allows clear evaluation of the importance of each of the Glu and Tyr residues. Catalytic activities of the recombinant proteins were measured in isolated membrane fractions from each culture. As shown in Fig. 4, the specific activities of E214A and Y221A enzymes were undetectable, whereas the activities of E215A, E216A, Y199A, Y212A, and Y247A were 29.2%, 35.4%, 56.1%, 9.2%, and 5.0% of the wild-type enzyme, respectively. This result indicates that E_{214} and Y_{221} are essential for the enzymatic reaction carried out by TvAOX. The reduced quinol oxidase activity in E_{215}, E_{216}, Y_{199}, Y_{212}, and Y_{247} mutants may be due to alteration of the native structure of the enzyme. It should be emphasized that these results were consistent with those from the plate and liquid cultures.

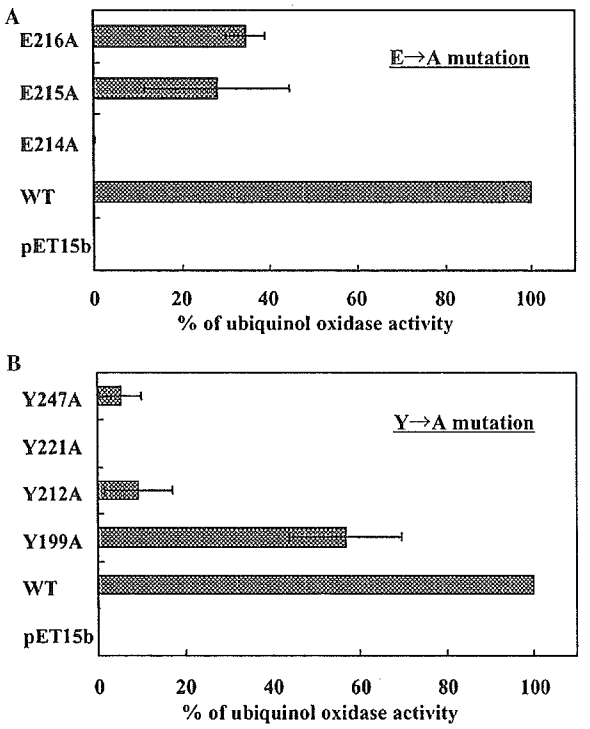

Fig. 4. Ubiquinol oxidase activity in membrane isolates from the *E. coli/ΔhemA* strains. The ubiquinol oxidase activity was compared between the mutant- and wild-type (WT)-expressing strains. A 995-μL mixture of membrane fraction in 50 mM Tris–HCl (pH 7.5) was preincubated for 3 min at 25 °C and then mixed with 5 μL of 150 μM ubiquinol-1 (molar extinction coefficient = 15,000) in ethanol to initiate the reaction. The absorbance change at 278 nm was used to determine the ubiquinol oxidase activity. The results show that, like cells expressing the empty vector (pET15b), the cells expressing the E214A and Y221A mutants had no enzyme activity.

Sensitivity of the mutants to AF

The antibiotic AF was isolated from the phytopathogenic fungus, *A. visiae*, and was found to specifically target the TAO, indicating that the site of inhibition is the same or close to the quinol substrate binding pocket [20]. In Figs. 2B and F, we showed that AF inhibited the growth of all *E. coli/ΔhemA* strains in the presence of active recombinant TvAOX. The IC_{50} values for AF were also determined in the ubiquinol oxidase activity assay using membrane preparations from all of the mutants. Basically, all of the mutants were very sensitive to AF. Most of the mutants had an IC_{50} value of 0.20 nM, similar to that of the wild-type enzyme, whereas E216A and Y247A mutations were less sensitive, with IC_{50} values of 0.60 and 0.55 nM, respectively. These results suggest that the residues mutated in this study are not directly involved in AF binding. We are currently performing more detailed investigations of the binding site for AF using random mutagenesis.

$E(X)_6Y$ motif in the AOX and the PTOX

In this study, we showed that the first Glu in the LEEEA motif, part of the third predicted helix region (P_{203} to R_{232}), is essential for enzymatic catalysis by TvAOX. Interestingly, the conserved Tyr residue (Tyr_{221}), which is separated by seven amino acids from the first Glu (Glu_{214}) in the triplet, is also indispensable for activity. We also found that the Y221A but not the Y199A mutation caused a complete loss of ubiquinol oxidase activity in TvAOX. This result is consistent with the findings of Albury et al. [3]. By studying the mutations of Tyr_{253} and Tyr_{275} to Phe in *S. guttatum* AOX, which correspond to mutations at Tyr_{199} and Tyr_{221} in TvAOX, they concluded that Tyr_{275} but not Tyr_{253} is essential for AOX activity. In the current studies, sequence alignment of the 50 AOXs and 10 PTOXs showed that this $E(X)_6Y$ motif is strictly conserved in AOX and PTOX.

The position of the conserved Tyr residue in this motif within a number of diiron carboxylate proteins reveals an interesting aspect of its possible function. In the second helix of the R2 protein of the normal class I ribonucleotide reductases, there is a diiron site that produces a stable Tyr free radical. This diiron site is situated six amino acids away from the iron-coordinating Glu residue [21]. Moreover, the bacterioferritin–ferritin–rubrerythrin class II diiron carboxylate proteins have also been found to contain a Tyr residue in the first helix region that is important for stabilization of the dinuclear irons and that is six amino acids away from the conserved Glu of the diiron binding motif [22]. Molecular modeling of

rat CLK-1, based on crystallographic data for several diiron carboxylate proteins, has predicted that Tyr_{29}, which is separated by six amino acids from the conserved Glu, contributes to the stabilization of the diiron center during the catalytic cycle [22].

Based on our amino acid alignment and enzymatic studies and according to the model of Anderson and Nordlund [14] (Fig. 1), it appears that the strictly conserved and essential Tyr residue in the $E(X)_6Y$ motif of the predicted third helix of AOXs and the PTOXs is located on the matrix side of the inner mitochondrial membrane. This is consistent with the idea that both oxidation of ubiquinol and reduction of molecular oxygen occur on the matrix side of the membrane, although the amino acids participating in these reactions have not yet been identified. As in other diiron carboxylate proteins having a helix structure, the Tyr residue could be a possible site of radical formation or iron stabilization essential for the activity of both enzymes [3,21].

Implications of the current findings

Trypanosoma vivax is a causative agent of African trypanosomiasis in livestock, and even in the absence of tsetse flies, it can be mechanically transmitted by various blood-sucking insects [23]. Because African trypanosomes can escape the host's immune system by mutating its cell surface antigen, the variant surface glycoprotein, the production of an effective vaccine has been problematic [6]. Thus, the major strategy against the parasites is centered on chemotherapy. The mitochondrion of the long slender form of African trypanosomes is considered to be a good target for chemotherapy because it has unique properties that are not found in mammals but are essential for parasite survival [24]. We previously reported the highly specific and effective anti-trypanosome inhibitor, AF. Our recent studies have shown that *T. vivax*-infected mice are cured with low dose of AF (Yabu et al., manuscript in preparation). The detailed information obtained from mutational analysis of the TvAOX active site will help to clarify the inhibitory mechanism of AF and should help to counteract the appearance of drug-resistant strains of *T. vivax*.

Acknowledgments

This study was supported by a Grant-in-Aid for scientific research on priority areas from the Japanese Ministry of Education, Science, Culture, and Sports (13226015 and 13854011) and for research on emerging and re-emerging infectious diseases from the Japanese Ministry of Health and Welfare. This study was also supported by the Pilot Applied Research Project for the Industrial Use of Space of the National Space Development Agency of Japan (NASDA) and the Japan Space Utilization Promotion Center (JSUP). The authors like to acknowledge Drs. K. Nagai, T. Hosokawa, and N. Minagawa for helpful discussions.

References

[1] A.E. McDonald, G.C. Vanlerberghe, Branched mitochondrial electron transport in the animalia: presence of alternative oxidase in several animal phyla, Life 56 (2004) 333–341.
[2] C. Affeurtit, M.S. Albury, P.G. Crichton, A.L. Moore, Exploring the molecular nature of alternative oxidase regulation and catalysis, FEBS Lett. 510 (2002) 121–126.
[3] M.S. Albury, C. Affourtit, P.G. Crichton, A.L. Moore, Structure of plant alternative oxidase: site-directed mutagenesis provides new information on the active site and membrane topology, J. Biol. Chem. 277 (2002) 1190–1194.
[4] T. Suzuki, T. Hashimoto, Y. Yabu, Y. Kido, K. Sakamoto, C. Nihei, M. Hato, S. Suzuki, Y. Amano, K. Nagai, T. Hosokawa, N. Minagawa, N. Ohta, K. Kita, Direct evidence for cyanide-insensitive quinol oxidase (alternative oxidase) in apicomplexan parasite *Cryptosporidium parvum*: phylogenetic and therapeutic implications, Biochem. Biophys. Res. Commun. 313 (2004) 1044–1052.
[5] Y. Fukai, H. Amino, H. Hirawake, Y. Yabu, N. Ohta, N. Minagawa, S. Sakajo, A. Yoshimoto, K. Nagai, S. Takamiya, S. Kojima, K. Kita, Functional expression of the AF-sensitive *Trypanosoma brucei brucei* alternative oxidase in the cytoplasmic membrane of *Escherichia coli*, Comp. Biochem. Physiol. C 124 (1999) 141–148.
[6] T. Suzuki, C. Nihei, Y. Yabu, T. Hashimoto, M. Suzuki, A. Yoshida, K. Nagai, T. Hosokawa, N. Minagawa, S. Suzuki, K. Kita, N. Ohta, Molecular cloning and characterization of *Trypanosoma vivax* alternative oxidase (AOX) gene, a target of the trypanocide ascofuranone, Parasitol. Int. 53 (2004) 235–245.
[7] N. Minagawa, S. Sakajo, T. Komiyama, A. Yoshimoto, Essential role of ferrous iron in cyanide-resistant respiration in *Hansenula anomala*, FEBS Lett. 267 (1990) 114–116.
[8] W.U. Ajayi, M. Chaudhuri, G..C. Hill, Site-directed mutagenesis reveals the essentiality of the conserved residues in the putative diiron active site of the trypanosome alternative oxidase, J. Biol. Chem. 277 (2002) 8187–8193.
[9] D.A. Berhold, P. Stenmark, Membrane-bound diiron carboxylate proteins, Annu. Rev. Plant Biol. 54 (2003) 497–517.
[10] D. Wu, D.A. Wright, C. Wetzel, D.F. Voytas, S. Rodermel, The IMMUTANS variegation locus of *Arabidopsis* defines a mitochondrial alternative oxidase homolog that functions during early chloroplast biogenesis, Plant Cell 11 (2004) 43–55.
[11] P. Carol, D. Stevenson, C. Bisanz, J. Breitenbach, G. Sandmann, R. Mache, G.. Coupland, M. Kuntz, Mutations in the Arabidopsis gene *IMMUTANS* cause a variegated phenotype by inactivating a chloroplast terminal oxidase associated with phytoene desaturation, Plant Cell 11 (1999) 57–68.
[12] A.E. McDonald, S. Amirsadeghi, G.C. Vanlerberghe, Prokaryotic orthologues of mitochondrial alternative oxidase and plastid terminal oxidase, Plant Mol. Biol. 53 (2003) 865–876.
[13] A. Atteia, R. van Lis, J.J. van Hellemond, A.G. Tielens, W. Martin, K. Henze, Identification of prokaryotic homologues indicates an endosymbiotic origin for the alternative oxidases of mitochondria (AOX) and chloroplasts (PTOX), Gene 330 (2004) 143–148.
[14] M.E. Andersson, P.A. Nordlund, Revised model of the active site of alternative oxidase, FEBS Lett. 449 (1999) 17–22.
[15] M.R. Aluru, A.R. Rodermel, Control of chloroplast redox by the IMMUTANS terminal oxidase, Physiol. Plantarum 120 (2004) 4–11.

[16] M. Chaudhuri, W. Ajayi, G.C. Hill, Biochemical and molecular properties of the *Trypanosoma brucei* alternative oxidase, Mol. Biochem. Parasitol. 95 (1998) 53–68.
[17] N. Minagawa, Y. Yabu, K. Kita, K. Nagai, N. Ohta, K. Meguro, S. Sakajo, A. Yoshimoto, An antibiotic, AF, specifically inhibits respiration and in vitro growth of long slender bloodstream forms of *Trypanosoma brucei brucei*, Mol. Biochem. Parasitol. 84 (1997) 271–280.
[18] J.D. Thompson, D.G. Higgins, T.J. Gibson, CLUSTAL W: improving the sensitivity of progressive multiple sequence alignment through sequence weighting, positions-specific gap penalties and weight matrix choice, Nucleic Acids Res. 22 (1994) 4673–4680.
[19] Y. Fukai, C. Nihei, Y. Yabu, T. Suzuki, N. Ohta, N. Minagawa, K. Nagai, K. Kita, Strain-specific difference in amino acid sequences of trypanosome alternative oxidase, Parasitol. Int. 51 (2002) 195–199.
[20] C. Nihei, Y. Fukai, K. Kawai, A. Osanai, Y. Yabu, T. Suzuki, N. Ohta, N. Minagawa, K. Nagai, K. Kita, Purification of active recombinant trypanosome alternative oxidase, FEBS Lett. 538 (2003) 35–40.
[21] M. Hogbom, P. Stenmark, N. Voevodskaya, G. McClarty, A. Graslund, P. Nordlund, The radical site in Chlamydial ribonucleotide reductase defines a new R2 subclass, Science 305 (2004) 245–248.
[22] S. Rea, CLK-1/Cop7p is a DMQ mono-oxygenase and a new member of the diiron carboxylate protein family, FEBS Lett. 509 (2001) 389–394.
[23] P.R. Gardiner, Recent studies of the biology of *Trypanosoma vivax*, Adv. Parasitol. 28 (1989) 229–317.
[24] K. Kita, C. Nihei, E. Tomitsuka, Parasite mitochondria as drug target: diversity and dynamic changes during the life cycle, Curr. Med. Chem. 10 (2003) 2535–2548.

Parasite Mitochondria as a Target of Chemotherapy

Inhibitory Effect of Licochalcone A on the *Plasmodium falciparum* Respiratory Chain

FUMIKA MI-ICHI,[a] HIROKO MIYADERA,[a] TAMAKI KOBAYASHI,[a] SHINZABURO TAKAMIYA,[b] SEIJI WAKI,[c] SUSUMU IWATA,[d] SHOJI SHIBATA,[e] AND KIYOSHI KITA[a]

[a]*Department of Biomedical Chemistry, Graduate School of Medicine, The University of Tokyo, Hongo, Bunkyo-ku, Tokyo 113-0033, Japan*

[b]*Department of Molecular and Cellular Parasitology, Juntendo University, School of Medicine, Hongo, Bunkyo-ku, Tokyo 113-8421, Japan*

[c]*Gunma Prefectural College of Health Sciences, Maebashi, Gunma 371, Japan*

[d]*Research Laboratory of Minophagen Pharmaceutical Co. Zama-shi, Kanagawa 228, Japan*

[e]*Shibata Laboratory of Natural Medicinal Materials, Minophagen Pharmaceutical Co. Yotsuya, Shinjyuku-ku, Tokyo 160, Japan*

ABSTRACT: **Parasites have exploited unique energy metabolic pathways as adaptations to the natural host habitat. In fact, the respiratory systems of parasites typically show greater diversity in electron transfer pathways than do those of host animals. These unique aspects of parasite mitochondria and related enzymes may represent promising targets for chemotherapy. Natural products have been recognized as a source of the candidates of the specific inhibitors for such parasite respiratory chains. Chalcones was recently evaluated for its antimalarial activity *in vitro* and *in vivo*. However, its target is still unclear in malaria parasites. In this study, we investigated that licochalcone A inhibited the bc_1 complex (ubiquinol-cytochrome *c* reductase) as well as complex II (succinate ubiquinone reductase, SQR) of *Plasmodium falciparum* mitochondria. In particular, licochalcone A inhibits bc_1 complex activity at very low concentrations. Because the property of the *P. falciparum* bc_1 complex is different from that of the mammalian host, chalcones would be a promising candidate for a new antimalarial drug.**

KEYWORDS: **parasite; mitochondria; chemotherapy; plasmodium; succinate; ubiquinone; licochalcone**

Address for correspondence: Kiyoshi Kita, Department of Biomedical Chemistry, Graduate School of Medicine, The University of Tokyo, Hongo, Bunkyo-ku, Tokyo 113-0033, Japan. Voice: +81-3-5841-3526; fax: +81-3-5841-3444.
kitak@m.u-tokyo.ac.jp

Ann. N.Y. Acad. Sci. 1056: 46–54 (2005). © **2005 New York Academy of Sciences.**
doi: 10.1196/annals.1352.037

INTRODUCTION

Biological systems for energy metabolism are essential for the survival, continued growth, and reproduction of all living organisms, including parasites. A key energy-transducing mechanism in this regard is the aerobic respiratory chain, a pathway mediating electrogenic translocation of protons out of mitochondrial or bacterial membranes. This generates the proton motive force that drives ATP synthesis by F_oF_1-ATPase, a mechanism that has essentially remained unchanged from bacteria to human mitochondria. Parasites, however, have exploited unique energy metabolic pathways as adaptations to the natural host habitat. In fact, the respiratory systems of parasites typically show greater diversity in electron transfer pathways than those of host animals. These unique aspects of parasite mitochondria may represent promising targets for chemotherapy.[1]

Our recent findings suggested that antirespiratory drugs affect parasite survival. A novel compound, nafuredin, inhibits NADH-fumarate reductase activity of *Ascaris suum* mitochondria, a unique anaerobic electron transport system in helminth mitochondria.[2] Also in trypanosome, cyanide-insensitive oxidase (trypanosome alternative oxidase [TAO]) has been targeted for the development of the antitrypanosomal drug ascofranone, because it does not exist in the host.[3] Thus, parasite mitochondria have become a focus of chemotherapy.

Malaria is one of the most serious infectious diseases in the developing world. Mortality associated with malaria is estimated at more than 1 million deaths per year and is mainly caused by the erythrocytic stage cells of *Plasmodium falciparum*.[4] Development of new antimalarial drugs is urgently required, because drug-resistant parasites are widespread.[5] Much research has been undertaken to explore the potential of new antimalarials and their targets. In *Plasmodium*, the differences between the mitochondria of malaria parasites and those of the host are also expected to be the target for chemotherapy.[6] The inhibition site of atovaquone, which is a recently developed antimalarial agent, is considered to be the ubiquinone oxidation site of cytochrome *b* in the bc_1 complex of the parasite mitochondria.[7,8] Atovaquone is effective against chloroquine-resistant strains and is already being used for therapy in epidemic regions in Africa and Thailand.[9] In addition, complex II was shown to be an essential component for parasite survival by antisense DNA analysis. Antisense DNA for Ip inhibited the growth of the malaria parasite.[10] These data clearly indicate that the bc_1 complex and complex II would be the target of chemotherapy for malaria.

As these enzymes have quinone-binding sites (FIG. 1), ubiquinone plays an important role in the respiratory chain of *Plasmodium* mitochondria.[6] It is a point of contact between pyrimidine metabolism and energy metabolism, both of which are essential metabolic systems for malaria parasites. By targeting this point, therefore, it may be possible to inhibit simultaneously these two important metabolic systems. Because many antimalarial agents contain a quinone structure, the enzymes mediating the electron transfer between the enzymes and ubiquinone are considered to be good targets.[11]

Chalcones, which are a promising group of flavonoids for antitumor-promoting activity, were recently evaluated for their antimalarial activity *in vitro* and *in vivo*.[12] These compounds were originally isolated from Xin-jiang licorice and have been shown to have various biological effects, such as antitumor, antibacterial, antituber-

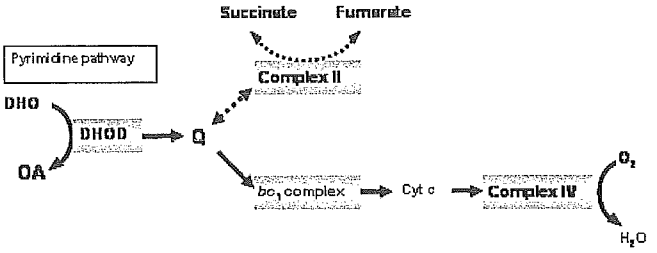

FIGURE 1. Respiratory chain of *P. falciparum* mitochondria.

culous, antiviral, antiprotozoal, and others.[13,14] However, their target and the inhibition mechanism were still unclear. This lack of molecular understanding of the target and mechanisms of action has impeded the development of efficient antimalarial drugs despite the many synthetic analogs, such as alkoxylated, hydroxylated, oxygenated, and quinolinyl chalcones, that have been synthesized.[15–18] A cysteine proteinase, falcipain, was evaluated as the target of chalcone analogs, but it was concluded in the same report that the antimalarial activity of chalcones was probably not due to the inhibition of falcipain and may follow a different mechanism because the antimalarial activity did not correlate well with the inhibition of the enzyme.[16]

In *Leishmania,* fumarate reductase (FRD) activity of complex II was characterized as the target of chalcone.[19] Generally, FRD activity is essential for the anaerobic respiratory chain of many parasites. Since complex II has a quinone-binding site, there is a possibility that complex II is a target also in *Plasmodium*. However, there has been no experimental evidence of the effect of chalcones on the respiratory chain of *Plasmodium,* because it was difficult to prepare the active mitochondria from *Plasmodium* spp. To solve this problem, we have established a protocol to prepare the active mitochondria from *P. falciparum,* showing high and reproducible respiratory enzyme activities.[10,20]

In this study, we showed that licochalcone A inhibited the bc_1 complex as well as complex II of *P. falciparum* mitochondria. The bc_1 complex was more sensitive to licochalcone A and its IC_{50} was 0.10 μM. Because the property of the *P. falciparum* bc_1 complex is different from that of mammals, chalcones should be a promising candidate for a new antimalarial drug.

MATERIAL AND METHODS

Culture

The *P. falciparum* parasite lines used were the Honduras-1. The parasites were cultured as described by Trager and Jensen in A(+) erythrocytes at 3% hematocrit in medium RPMI 1640 (Sigma), supplemented with 25 mM HEPES, 10 mM glucose, 0.32 mM hypoxanthine, and 10% (v/v) heat-inactivated human plasma, and in an atmosphere of 90% N_2, 5% O_2, and 5% CO_2. The growth medium was replaced